Universities of Leeds, Sheffield and York
http://eprints.whiterose.ac.uk/

Published paper
Griffo, A. and Lauria, D. (2008) *Two-leg three-phase inverter control for STATCOM and SSSC applications,* IEEE Transactions on Power Delivery, Volume 23 (1), 361-370.

Two-Leg Three-Phase Inverter Control for STATCOM and SSSC Applications

Antonio Griffo and Davide Lauria

Abstract—**Flexible ac transmission systems (FACTS) devices are attracting an increasing interest both in power system academic research and in electric utilities for their capabilities to improve steady-state performance as well as system stability. Several converter topologies for FACTS applications have been proposed in the recent literature, even if those based upon voltage source inverters (VSI) seem to be more attractive due to their intrinsic capability to rapidly respond to network changes such as perturbations subsequent to a fault and their property of being immune to resonance problem. In this paper, a new topology for inverter-based FACTS is proposed. This configuration, employing a two-leg three-phase inverter is employed for both series and parallel-connected reactive power compensators. The converter utilizes a modular topology for allowing a satisfaction of electronic components rating. A control strategy based on variable structure control technique with sliding mode is employed to track appropriate reference quantities. Design and control, as well as good tracking performances, are also verified through numerical simulations.**

Index Terms—**Flexible ac transmission systems, static synchronous compensator (STATCOM), static synchronous series compensator (SSSC), variable structure control.**

I. INTRODUCTION

POWER system regulation has historically played a vital role for secure operation of electrical power systems. The interest towards the identification of the best control actions which could improve dynamic behaviour is further increased in modern power systems since the deregulation could involve stressed operating conditions. The evolution in power electronic devices along with developments in control theory have allowed the design and implementation of structural controllers known as flexible ac transmission systems (FACTS), which are emerging as a viable technology for the improvement of power systems dynamic behavior. The benefits arising from FACTS devices are widely appreciated and are not restricted to the increase in power flows and stability margins [1]–[3], but also extend to power oscillations damping [4], [5].

Many devices have been proposed in the past within the FACTS family, some of them based on thyristor switched reactors like the TCSC and StaticVar [6], while others, like the static compensator (STATCOM) [7], the static synchronous series compensator (SSSC) [8], the unified power flow controller (UPFC) [9], and the superconducting magnetic energy storage systems (SMES) [10], employ power electronic converters. This latter choice guarantees the best flexibility in control and rapidity of response. Several power converter topologies have been proposed for the implementation of FACTS devices, such as those based on voltage-source converters [11] and current-source converters [12]. Among voltage-source converters, line-frequency switching has been preferred to pulsewidth modulation (PWM) due to the past unavailability of high switching-frequency power devices with high power-handling capabilities. In order to achieve lower harmonic distortion, multipulse converter are employed, such as the 24- and 48-pulse converters [13]–[15]. Magnetic interfaces constituted by complex zig-zag phase shifting transformers are required for interfacing multipulse inverters with transmission network in order to counteract low order harmonics. With the use of multilevel converters [16], the necessity of complex coupling transformers could be avoided, at the expense of a greater complexity in control. Comprehensive circuit-level comparisons, along with advantages and drawbacks of several common arrangements for high-power converters, are presented in [11] and [17].

Several improvements in power semiconductor devices have been reported recently. Insulated gate-commutated thyristors (IGCTs) [18], [19] have been proposed and are already commercially available for high power operations with switching frequency in the kilohertz range. The emitter turn-off thyristor (ETO) promises to be a viable technology for very high power and high frequency PWM operation [20]–[22]. These progresses are making PWM operation a competitive and effective alternative to line-frequency commutated control structure which are currently employed.

Power converters can be regarded as variable structure systems due to their switching operation. Sliding-mode control for this type of system has gained widespread attention in the relevant literature due to its simplicity and intrinsic robustness against disturbances [23], [24]. Sliding-mode control is thus an effective alternative to classical PWM techniques, provided that sufficiently high switching-frequency devices are available. A viable solution to the problem of high frequency switching of high current levels is the employment of a number of parallel connected converters, controlled in such a way as to guarantee a balanced current sharing among them. In this paper, a converter based on the parallel connection of basic building blocks constituted by two-leg three-phase converter, for both parallel and series compensation, is described. This arrangement can provide an alternative topology for STATCOM and SSSC devices.

A. Griffo is with the Department of Electronic and Electrical Engineering, University of Sheffield, Sheffield S1 3JD, U.K. (e-mail: A.Griffo@sheffield.ac.uk).

D. Lauria is with the Department of Electrical Engineering, Università degli Studi di Napoli Federico II, 80125 Napoli, Italy (e-mail: davide.lauria@unina.it).
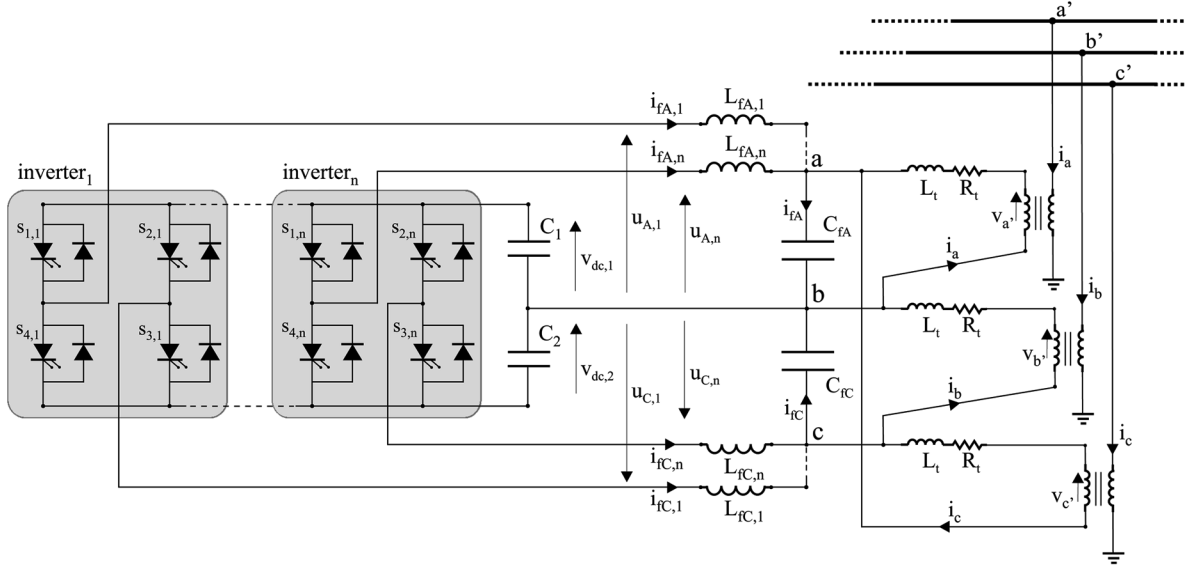
Fig. 1. Proposed converter topology and parallel connection with the transmission network.

While the STATCOM based on the proposed converter is employed for stabilizing voltage at the point of common coupling with the network, the SSSC is employed for both capacitive and inductive compensation of a transmission line. Both problems can be rearranged into the problem of tracking a reference reactive power. This problem is thereafter translated into the task of tracking a reference voltage which is effectively achieved with a sliding mode controller, which also tackles the problem of balanced current sharing among the parallel connected converters. The paper is structured as follows: converter configuration and its application for STATCOM operation is presented in Section II, along with mathematical derivations of both references quantities and control action. Series connection for SSSC operation is described in Section III. In Section IV, results of numerical simulations are reported, showing good tracking performances along with simplicity in design and control. The conclusion is presented in Section V.

II. CONVERTER TOPOLOGY, STATCOM OPERATION, AND CONTROL

The topology of the proposed converter is illustrated in Fig. 1, as well as its shunt connection with the transmission network through a Δ-Y transformer. The converter is constituted by the parallel connection of n two-leg three-phase inverters. LC filters are connected between each inverter output and the coupling transformer, in order to contribute to the smoothing of output voltages. The basic building block has been proposed as a component minimized topology for variable-speed induction motor drives [25], [26] and as a coupled rectifier/inverter system [27]. A three-level NPC variant has also been proposed for active filtering application [28].

Assuming a balanced three-phase operation, the converter output voltage $\bar{V}_{ab}$ is given by

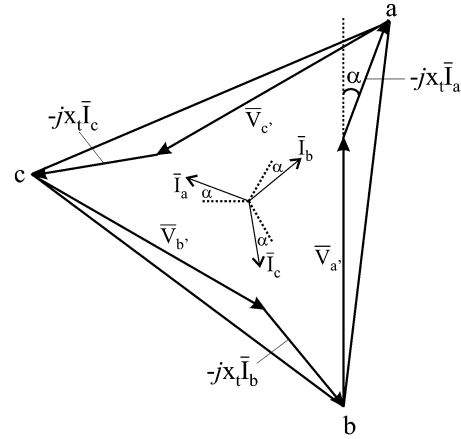$$\bar{V}_{ab} = \bar{V}_{a'} - jx_t\bar{I}_a \qquad (1)$$

Fig. 2. Phasor diagram illustrating STATCOM operation in capacitive compensation mode.

where $\bar{V}_{a'}$ is the transmission network phase a p.u. voltage at the point of common coupling, $\bar{I}_a$ is the STATCOM phase a p.u. current and x_t the coupling transformer leakage reactance. Leakage resistance has been neglected for the sake of simplicity. Voltages $\bar{V}_{ca}$ and $\bar{V}_{bc}$ can be derived analogously, and are equal to $\bar{V}_{ab}$ phase shifted by $2/3\pi$ and $4/3\pi$ rad, respectively, as illustrated by the phasor diagram in Fig. 2.

For the STATCOM to operate as a capacitive compensator, the currents $\bar{I}_{a,b,c}$ drawn from the network should lead bus voltages $\bar{V}_{a',b',c'}$ by $\pi/2$ rad, while the currents should lag $\pi/2$ rad behind the voltages when inductive compensation is required. Assuming as a reference the phase of $\bar{V}_{a'}$, the STATCOM reference phase current is then

$$\bar{I}_a^{\mathrm{ref}} = I_a^{\mathrm{ref}}e^{j(\pi/2-\alpha)}. \qquad (2)$$

A phase displacement by an angle α is necessary for the STATCOM to draw sufficient active power as to compensate
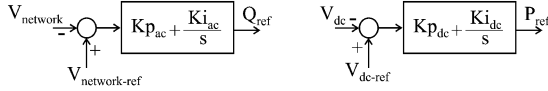
Fig. 3. Ac and dc control systems.

for losses in semiconductor devices and coupling transformer, thus maintaining dc voltage at a specified level. The magnitude of the reference current, as well as angle α, can be derived by the reference values of active and reactive power as

$$I_a^{\text{ref}} = I^{\text{ref}} = \frac{\sqrt{P_{\text{ref}}^2 + Q_{\text{ref}}^2}}{V_{a',b',c'}} \tag{3}$$

$$\alpha = \frac{\pi}{2} - \tan^{-1} \frac{Q_{\text{ref}}}{P_{\text{ref}}}. \tag{4}$$

Active and reactive power reference can either be fixed or dynamically adjusted as to regulate some network quantities. The most common STATCOM operation is voltage regulation at the point of common coupling. With this aim in mind, two simple PI regulators, as reported in Fig. 3, are adopted in the paper. The difference between network voltage magnitude and a reference is passed through a PI controller which determines the amount of reactive power compensation required. A regulation droop is usually present in practical arrangements and can be easily added. Another PI regulator maintains dc voltage at a specified level, by determining the amount of active power necessary for converter losses compensation. More complex control schemes, which could further enhance system dynamic behavior, are equally possible but, since the main focus is on the tracking capabilities of the proposed converter and control, only the simplest are presented.

Reference values for magnitude and phase of converter output voltage are then

$$|\bar{V}_{ab}^{\text{ref}}| = \sqrt{\left(V_{a'} + x_t I_a^{\text{ref}} \cos \alpha\right)^2 + \left(x_t I_a^{\text{ref}} \sin \alpha\right)^2} \tag{5}$$

$$\angle \bar{V}_{ab}^{\text{ref}} = \angle \bar{V}_{a'} - \tan^{-1} \frac{x_t I_a^{\text{ref}} \sin \alpha}{V_{a'} + x_t I_a^{\text{ref}} \cos \alpha}. \tag{6}$$

$\bar{V}_{ca}$ and $\bar{V}_{bc}$ can be derived by phase shifting $\bar{V}_{ab}$ by $2/3\pi$ and $4/3\pi$ rad, respectively. In practical applications, a phase-locked loop (PLL) is necessary to synchronize with the network voltage.

Time-domain converter equations are presented in the following.

A. Converter Equations

Voltages on ac filter capacitances v_{ab}, v_{cb} which constitute the output to be regulated are described by

$$\frac{dv_{ab}}{dt} = \frac{1}{C_{fA}} i_{fA}$$

$$\frac{dv_{cb}}{dt} = \frac{1}{C_{fC}} i_{fC} \tag{7}$$

where

$$i_{fA} = \sum_{k=1}^{n} i_{fA,k} + i_a - i_c$$

$$i_{fC} = \sum_{k=1}^{n} i_{fC,k} + i_c - i_b. \tag{8}$$

Equations for currents in filter inductances are

$$\frac{di_{fA,k}}{dt} = \frac{1}{L_{fA,k}} (u_{A,k} - v_{ab})$$

$$\frac{di_{fC,k}}{dt} = \frac{1}{L_{fC,k}} (u_{C,k} - v_{cb}) \quad k \in \{1, \ldots, n\}. \tag{9}$$

The control inputs $u_{A,k}, u_{C,k}$ to LC filters are given by

$$u_{A,k} = s_{1,k} v_{dc,1} - s_{4,k} v_{dc,2}$$

$$u_{C,k} = s_{2,k} v_{dc,1} - s_{3,k} v_{dc,2} \tag{10}$$

where for the k-th inverter

$$s_{j,k} = \begin{cases} 1, & \text{if the } j - \text{th switch is on} \\ 0, & \text{if the } j - \text{th switch is off} \end{cases} \quad j \in \{1, \ldots, 4\}. \tag{11}$$

Currents in the primary of the coupling transformer are described by

$$\frac{di_a}{dt} = \frac{1}{L_t} (-R_t i_a - v_{ab} + v_{a'})$$

$$\frac{di_b}{dt} = \frac{1}{L_t} (-R_t i_b + v_{cb} + v_{b'})$$

$$\frac{di_c}{dt} = \frac{1}{L_t} (-R_t i_c + v_{ab} - v_{cb} + v_{c'}). \tag{12}$$

Equations (7)–(12) can be easily rearranged in the state-space form as

$$\dot{\mathbf{x}} = \mathbf{A}\mathbf{x} + \mathbf{B}\mathbf{u} + \mathbf{D}\mathbf{d}$$

$$\mathbf{y} = \mathbf{C}\mathbf{x} \tag{13}$$

where the state variables $\mathbf{x}$ and the controllable and uncontrollable inputs $\mathbf{u}, \mathbf{d}$, respectively, are given by

$$\mathbf{x} = [v_{ab}, v_{cb}, i_{fA,n}, \ldots, i_{fA,1}, i_{fC,n}, \ldots,$$
$$i_{fC,1}, i_a, i_b, i_c]^\top$$
$$\mathbf{u} = [u_{A,n}, \ldots, u_{A,1}, u_{C,n}, \ldots, u_{C,1}]^\top$$
$$\mathbf{d} = [v_{a'}, v_{b'}, v_{c'}]^\top \tag{14}$$

and the output $\mathbf{y}$ is

$$\mathbf{y} = [v_{ab}, v_{cb}]^\top. \tag{15}$$

Proper operation is achieved by regulating v_{ab}, v_{cb} to their respective reference values given by

$$v_{ab}^{\text{ref}} = |\bar{V}_{ab}^{\text{ref}}| \sin \left(\omega t + \angle \bar{V}_{ab}^{\text{ref}}\right)$$
$$v_{cb}^{\text{ref}} = |\bar{V}_{cb}^{\text{ref}}| \sin \left(\omega t + \angle \bar{V}_{cb}^{\text{ref}}\right)$$
$$= |\bar{V}_{ab}^{\text{ref}}| \sin \left(\omega t + \angle \bar{V}_{ab}^{\text{ref}} + \pi/3\right) \tag{16}$$
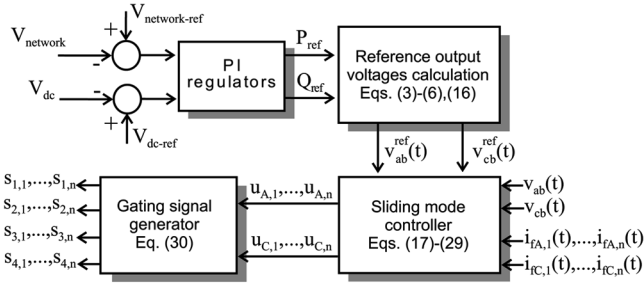
Fig. 4. Proposed control strategy for the converter in STATCOM operation.

by properly controlling $u_{A,i}, u_{C,i}, i = 1, \ldots, n$ acting on switches gate signals $s_{1,i}, s_{2,i}, s_{3,i}, s_{4,i}, i = 1, \ldots, n$. The whole control strategy is illustrated in Fig. 4.

B. Variable Structure Control

Due to the switching action of power devices, power converters naturally belong to the class of variable structure systems, whose structure changes according to some control law. Variable structure control (VSC) is a feedback control action widely employed for this kind of systems. VSC have been proposed for a variety of mechanical and electrical systems, also including power converters [29], power systems [30], and electrical drives [31]. The design of a VSC for a given system entails the choice of a switching control law with the aim of forcing system's state trajectory towards a properly designed sliding surface in the state space, described by $\Sigma(\mathbf{x}, t) = \mathbf{0}$. Once the sliding surface is reached, the VS controller must preserve the motion of system's trajectory on it, giving rise to the so-called sliding mode. Control objectives should be taken into account for an appropriate design of the sliding surface. In the present case, the goals of the controller can be itemized as follows.

1) Regulation of output voltages v_{ab}, v_{cb}.
2) Balanced current sharing among parallel connected inverters.

Keeping these aims in mind, the following sliding surface is proposed, utilizing the circular chain control strategy from [32]

$$\Sigma(\mathbf{x}, t) = [\sigma_{A,1}, \ldots, \sigma_{A,n}, \sigma_{C,1}, \ldots \sigma_{C,n}s]^\top = \mathbf{0} \quad (17)$$

where

$$\sigma_{A,h} = \left(v_{ab} - v_{ab}^{\mathrm{ref}}\right) + \alpha \left(\frac{dv_{ab}}{dt} - \frac{dv_{ab}^{\mathrm{ref}}}{dt}\right)$$
$$+ \beta(i_{fA,h} - i_{fA,k})$$
$$\sigma_{C,h} = \left(v_{cb} - v_{cb}^{\mathrm{ref}}\right) + \alpha \left(\frac{dv_{cb}}{dt} - \frac{dv_{cb}^{\mathrm{ref}}}{dt}\right)$$
$$+ \beta(i_{fC,h} - i_{fC,k}) \quad (18)$$

with

$$k = n, \quad \text{if } h = 1$$
$$k = h - 1, \quad \text{if } h = 2, \ldots, n.$$

The first two terms on the right-hand side of (18) account for output voltage regulation, while the third accounts for balanced current sharing among parallel connected converters. The derivative term is added recognizing that the relative degree

(i.e., the order of the derivative of the output $\mathbf{y}$ required for the input $\mathbf{u}$ to appear explicitly [23]) is two [33]. Once the sliding surface is hit at $t = t_0$, the sliding mode occurs if and only if

$$\dot{\Sigma}(\mathbf{x}, t) = \frac{\partial \Sigma}{\partial \mathbf{x}} \cdot \dot{\mathbf{x}} + \frac{\partial \Sigma}{\partial t} = \mathbf{0}, \quad \forall t > t_0. \quad (19)$$

The equivalent control $\mathbf{u}_{\mathrm{eq}}$ given by:

$$\mathbf{u}_{\mathrm{eq}} = -\left(\frac{\partial \Sigma}{\partial \mathbf{x}} \cdot \mathbf{B}\right)^{-1} \cdot \left[\frac{\partial \Sigma}{\partial \mathbf{x}} \cdot (\mathbf{A}\mathbf{x} + \mathbf{D}\mathbf{d}) + \frac{\partial \Sigma}{\partial t}\right] \quad (20)$$

assuming $\det[(\partial \Sigma / \partial \mathbf{x}) \cdot \mathbf{B}] \neq 0$, describes an equivalent smooth feedback control that forces state trajectory of system (13) to stay on $\Sigma(\mathbf{x}, t) = \mathbf{0}$. Direct application of Proposition 1 in [34] to the present case demonstrates that a sliding mode exists if and only if $\forall \mathbf{x} \in \{\mathbf{x} : \Sigma = \mathbf{0}\}$ each component $u_{k,\mathrm{eq}}$ of the equivalent control $\mathbf{u}_{\mathrm{eq}}$ satisfies

$$-v_{dc,2} < u_{k,\mathrm{eq}} < v_{dc,1}. \quad (21)$$

This condition is fulfilled provided that voltages on dc capacitors are sufficiently high.

A reaching condition, sufficient for the trajectory of system's state to reach the sliding surface is

$$\left(\frac{d\Sigma}{dt}\right)^\top \cdot \Sigma < 0. \quad (22)$$

Condition (22) guarantees that the time derivative of the quadratic function

$$\mathcal{V} = 1/2 \Sigma^\top \cdot \Sigma \quad (23)$$

is negative definite, thus (23) qualifies as a Lyapunov function, demonstrating asymptotic stability of the state $\Sigma = \mathbf{0}$. In single-input control problem, actual control is derived as to fulfill condition (22). Since system (13) is a multi-input system, $2n$ actual controls would appear in a coupled manner in (23) thus making impossible to derive appropriate control actions. A linear time-invariant transformation:

$$\hat{\Sigma} = \Omega \cdot \Sigma \quad (24)$$

with Ω being a nonsingular matrix, chosen in order to transform the coupled multi-input control problem into $2n$ decoupled single input problems [24]. Motion on the sliding surface is not altered by transformation (24) since the equivalent control can be easily derived to be the same as (20). Furthermore, since Ω is nonsingular, $\Sigma = \mathbf{0} \Leftrightarrow \hat{\Sigma} = \mathbf{0}$. The candidate Lyapunov function is now

$$\hat{\mathcal{V}} = 1/2 \hat{\Sigma}^\top \cdot \hat{\Sigma} \quad (25)$$

whose time derivative is

$$\frac{d\hat{\mathcal{V}}}{dt} = \hat{\Sigma}^\top \cdot \Omega \cdot \left[\frac{\partial \Sigma}{\partial \mathbf{x}} \cdot (\mathbf{A}\mathbf{x} + \mathbf{B}\mathbf{u} + \mathbf{D}\mathbf{d}) + \frac{\partial \Sigma}{\partial t}\right]. \quad (26)$$

If Ω is chosen such that

$$\Omega \cdot \frac{\partial \Sigma}{\partial \mathbf{x}} \cdot \mathbf{B} = \mathbf{I} \iff \Omega = \left(\frac{\partial \Sigma}{\partial \mathbf{x}} \cdot \mathbf{B}\right)^{-1} \quad (27)$$
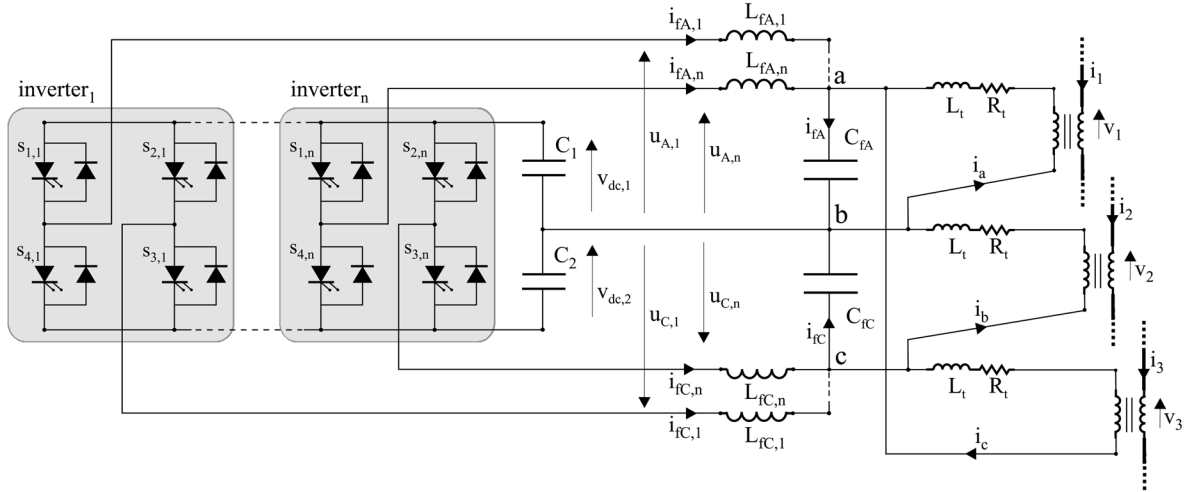
Fig. 5. Proposed converter topology and series connection with the transmission network.

where $\mathbf{I}$ is the identity matrix, then the time derivative of the function $\hat{\mathcal{V}}$ is

$$\frac{d\hat{\mathcal{V}}}{dt} = \hat{\Sigma}^\top \cdot \Omega \cdot \left[\frac{\partial \Sigma}{\partial \mathbf{x}} \cdot (\mathbf{Ax} + \mathbf{Dd}) + \frac{\partial \Sigma}{\partial t}\right] + \hat{\Sigma}^\top \cdot \mathbf{u}. \quad (28)$$

Expression for Ω in the present case is given in the Appendix.

A negative definite term is added to (28) if the control inputs are chosen as

$$u_{A,i}, u_{C,i} = \begin{cases} u^+ = & v_{dc,1}, & \text{if } \hat{\sigma}_i < 0 \\ u^- = & -v_{dc,2}, & \text{if } \hat{\sigma}_i > 0 \end{cases}. \quad (29)$$

Again, if dc voltages are sufficiently high, the reaching condition is satisfied, allowing sliding surface to be reached in finite time. Direct application of (29) would require an infinite switching frequency. In practical realization, an hysteresis band HB is considered in order to provide a finite and sufficiently low switching frequency. Gate signals $s_{1,k}, s_{2,k}, s_{3,k}, s_{4,k}$ for k-th inverter are easily derived from (10) and (29) as follows:

$$s_{1,i} = \begin{cases} 1, & \text{if } u_{A,i} = u^+ \\ 0, & \text{if } u_{A,i} = u^- \end{cases}$$

$$s_{4,i} = \begin{cases} 0, & \text{if } u_{A,i} = u^+ \\ 1, & \text{if } u_{A,i} = u^- \end{cases}$$

$$s_{2,i} = \begin{cases} 1, & \text{if } u_{C,i} = u^+ \\ 0, & \text{if } u_{C,i} = u^- \end{cases}$$

$$s_{3,i} = \begin{cases} 0, & \text{if } u_{C,i} = u^+ \\ 1, & \text{if } u_{C,i} = u^-. \end{cases} \quad (30)$$

III. CONVERTER TOPOLOGY, SSSC OPERATION AND CONTROL

The series connected converter is reported in Fig. 5. Apart from network connection, the converter and the filtering interface are the same as those already described for the STATCOM, thus their functions and equations will no be repeated here. The role of a series compensator is to provide a capacitive compensation for long transmission lines. As for STATCOM,
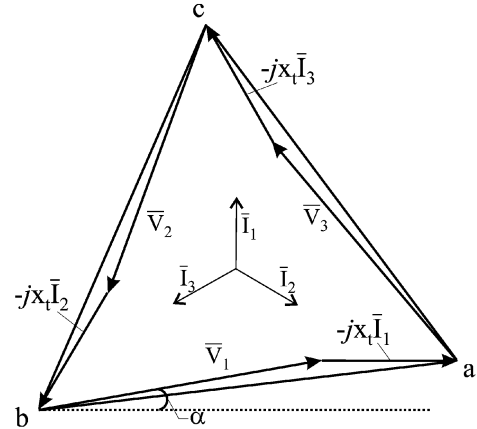

Fig. 6. Phasor diagram illustrating SSSC operation in capacitive compensation mode.

besides the main objective, supplementary controls could be added to provide additional capabilities such as current, power flow control, and damping of power oscillations. Although capacitive compensation is the most common operation of the SSSC, inductive compensation could be required in some circumstances, as well.

The phasor diagram reported in Fig. 6 illustrates the principle of capacitive compensation of SSSC, which injects three-phase voltages $\pi/2$ rad lagging line currents. Again, an angle $\alpha \neq 0$ is required for active power to flow into the converter in order to compensate for losses.

The following relationships, assuming balanced three-phase capacitive operation, are easily derived:

$$\bar{V}_{ab} = \bar{V}_1 - jx_t\bar{I}_a, \quad \bar{I}_a = \bar{I}_1. \quad (31)$$

Injected series voltage is

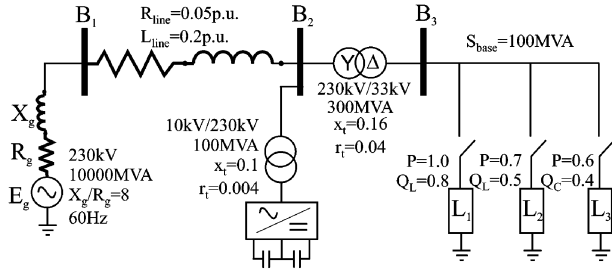$$\bar{V}_1 = -jx_{\text{comp}}|\bar{I}_1|e^{j(\angle \bar{I}_1 + \alpha)} \quad (32)$$

Fig. 7. The 230-kV test system for STATCOM simulation.

where x_{comp} is the desired compensator equivalent reactance. The magnitude and phase of converter output reference voltage are

$$\left|\bar{V}_{ab}^{\mathrm{ref}}\right| = \left|\bar{I}_1\right| \cdot \sqrt{(x_{\mathrm{comp}}\cos\alpha + x_t)^2 + (x_{\mathrm{comp}}\sin\alpha)^2} \tag{33}$$

$$\angle \bar{V}_{ab}^{\mathrm{ref}} = \angle \bar{I}_1 - \tan^{-1}\frac{x_t + x_{\mathrm{comp}}\cos\alpha}{x_{\mathrm{comp}}\sin\alpha}. \tag{34}$$

Again, $\bar{V}_{ca}$ and $\bar{V}_{bc}$ can be derived by phase shifting $\bar{V}_{ab}$ by $2/3\pi$ and $4/3\pi$ rad, respectively.

The control strategy for SSSC operation is the same as for STATCOM, as illustrated in Fig. 4, except for reference voltages derived from the desired equivalent series reactance.

IV. NUMERICAL SIMULATIONS

Numerical simulations for both compensators are reported in the following.

A. STATCOM

The test system reported in Fig. 7, adapted from [14], is employed for STATCOM simulation. It consists of a three-phase 230-kV ideal generator which feeds a load area through a transmission line and a step-down transformer. Three loads are switched sequentially, in order to provide different operating conditions. The proposed STATCOM is shunt connected to bus B_2 through a coupling transformer. Network data are reported in Fig. 7 while the converter and controller data are given in Appendix B. The converter utilized in numerical simulations is constituted by three parallel-connected inverters.

Load L_1 is connected from the beginning of simulation. At $t = 0.5$ s, a second inductive load L_2 is connected, while load L_3 which has a capacitive component is switched on at $t = 0.75$ s. At $t = 1$ s, loads L_1 and L_2 are both disconnected, leaving only the capacitive load, resulting in inductive operation of the STATCOM, as shown in Fig. 8, where both measured reactive power absorbed by the converter and its reference are shown.

The magnitude of voltage at the regulated bus B_2 and the magnitude of the current absorbed by the STATCOM are plotted in Fig. 9. Dc capacitor voltages and the angle α are shown in Fig. 10.

Phase a voltage and current at STATCOM output at the passage from capacitive (voltage lagging) to inductive (voltage leading) mode of operation are reported in Fig. 11.

Rms values of phase a output current of the three converters are reported in Fig. 12. Despite different values for filter induc-
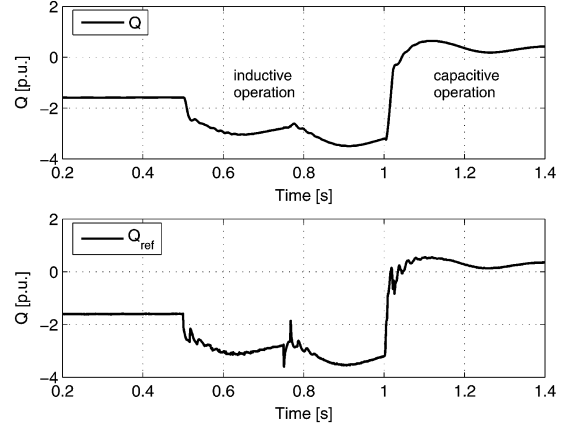

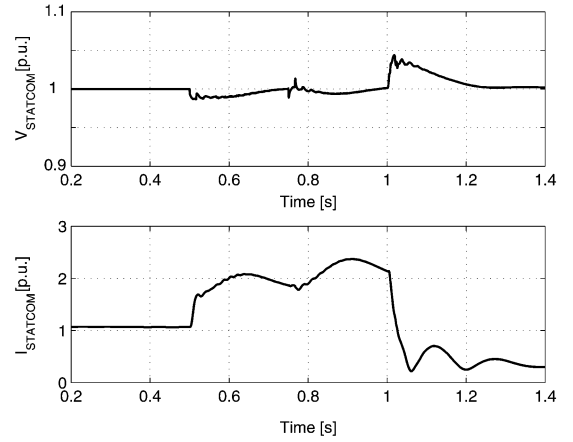Fig. 8. Actual (top) and reference (bottom) reactive power absorbed by the STATCOM.

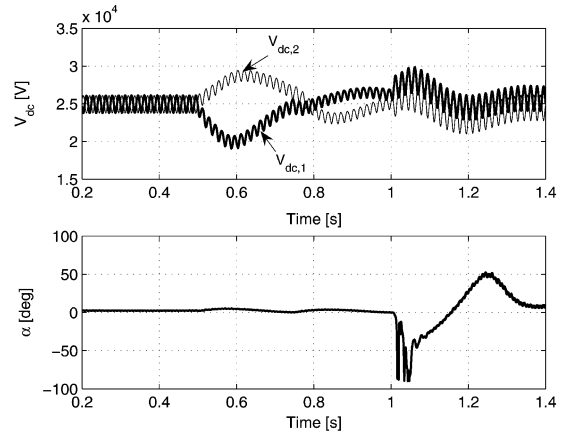Fig. 9. Magnitude of voltage (top) and current (bottom) at STATCOM output.

Fig. 10. DC capacitors voltages (top) and angle α (bottom).

tances, the current sharing is good. A higher number of parallel-connected inverters could be easily added to lower the current through each of them.

Voltage across filter capacitance v_{ab} and its reference v_{ab}^{ref} are reported in Fig. 13. Good tracking performances are obtained, resulting in low distortion of output voltage, as demonstrated by a THD value well below 0.1%, as shown in Fig. 14.
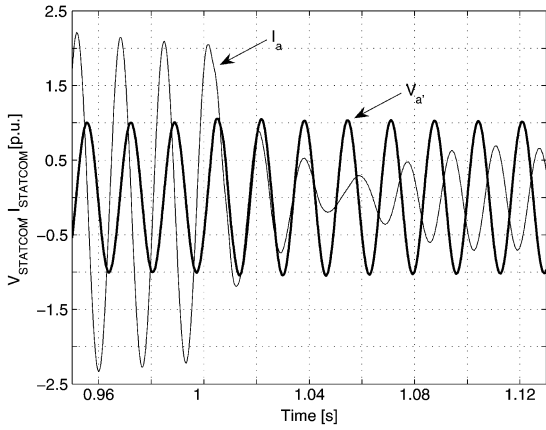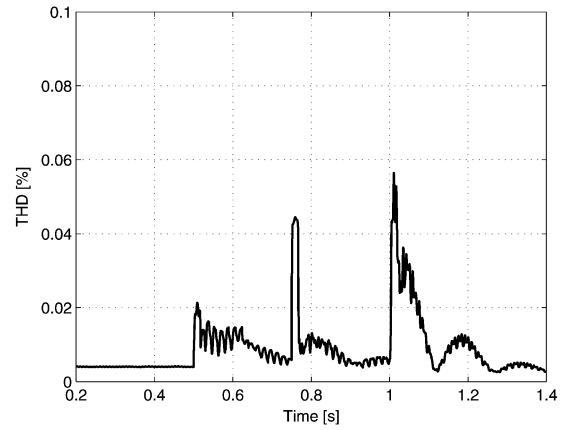
Fig. 11. Phase a STATCOM voltage and current.

Fig. 12. Current rms in filter inductances.
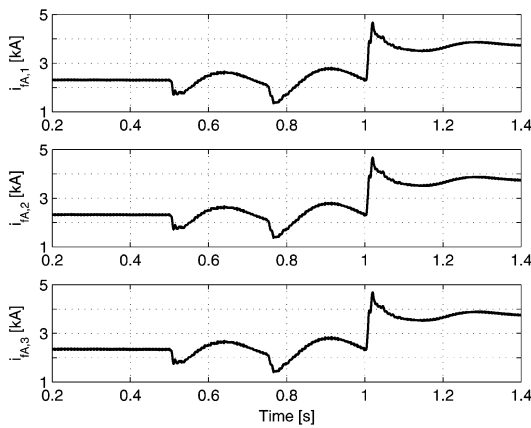

Fig. 13. v_{ab} (top) and v_{ab}^{ref} (bottom).

Sliding-mode control results in a variable switching frequency. By means of a running window, the number of commutations in a period has been evaluated and its maximum has been found to result in a maximum switching frequency as low as 1250 Hz.

B. SSSC

The test system used in SSSC simulations is reported in Fig. 15, [14]. Different operating conditions are tested by

Fig. 14. THD of bus B_2 voltage.

Fig. 15. 230-kV test system for SSSC simulation.

Fig. 16. SSSC equivalent reactance (top). Active and reactive power absorbed by SSSC (bottom).

switching on and off three loads and correspondingly changing the reference SSSC reactance. Load L_1 is connected from the beginning of the simulation while inductive load L_2 and capacitive load L_3 are switched on $t = 0.25$s and $t = 0.5$ s, respectively. At $t = 0.75$, loads L_1 and L_2 are both switched off while compensator goes into inductive compensation. Fig. 16 shows equivalent reference reactance and the active and reactive power absorbed by the compensator. Magnitude of injected voltage and current through SSSC are reported in Fig. 17, while Fig. 18 shows dc voltages and angle α. Phase 1 voltage and current of the SSSC, following the removal of inductive loads, thus determining the passage from capacitive to inductive compensation, is reported in Fig. 19. RMS values of phase 1 output current of the three converters are reported in Fig. 20. As for STATCOM good tracking performances
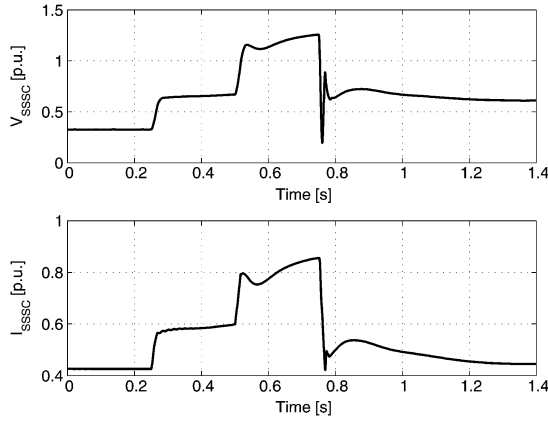
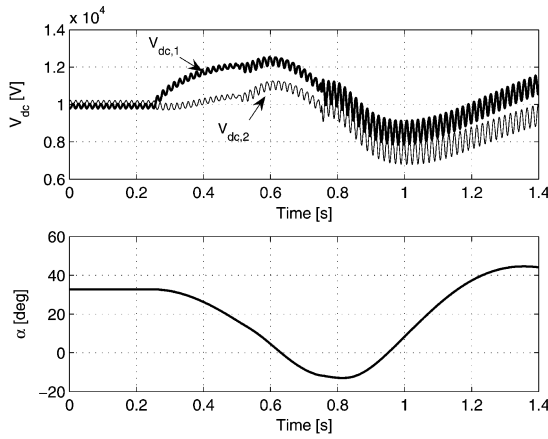Fig. 17. Magnitude of injected voltage (top) and current through SSSC (bottom).

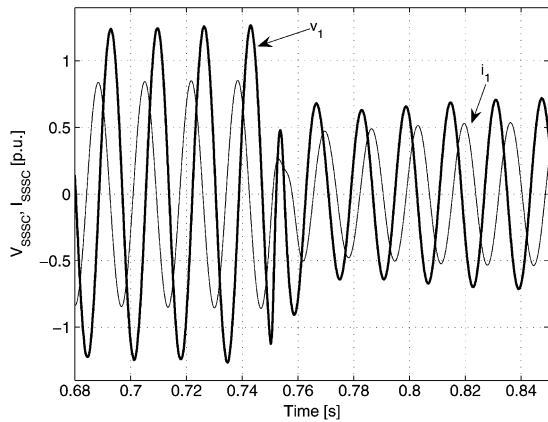Fig. 18. Dc capacitors voltages (top) and angle α (bottom).

Fig. 19. Phase 1 SSSC voltage and current.

are obtained with respect to output voltages with a switching frequency lower than 1250 Hz, which result in a THD level well below 0.1%.

V. CONCLUSION

In this paper, a converter constituted by the parallel operation of basic building blocks is utilized for both series and parallel reactive power compensation, thus proposing an alternative
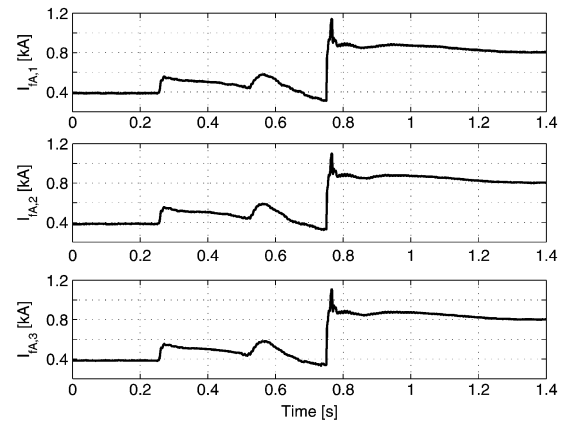

Fig. 20. Current rms in filter inductances.

topology for FACTS devices. Each building block is the most basic two-leg three-phase inverter constituted by four switches and a split capacitor. The compensation problem is translated into the task of tracking reference three-phase voltages at converter output. Recognizing the variable structure nature of the converter, the tracking problem is tackled by means of a sliding controller, which also provide a solution to the problem of a balanced current sharing among the two-leg parallel connected inverters. Numerical simulations are reported both for a STATCOM and a SSSC based on the proposed converter, showing simplicity both in control and converter topology, as well as effective tracking performance of the sliding controller.

APPENDIX A
LIST OF SYMBOLS

A list of symbols used throughout the paper is given next:

$\bar{V}_{ab}, \bar{V}_{bc}, \bar{V}_{ca}$	line to line compensator output voltages;
$\bar{V}_{ab}^{\mathrm{ref}}, \bar{V}_{cb}^{\mathrm{ref}}$	line to line compensator output reference voltages;
$\bar{V}_{a'}, \bar{V}_{b'}, \bar{V}_{c'}$	line to ground network voltages;
$\bar{I}_a, \bar{I}_b, \bar{I}_c$	currents drawn by the STATCOM;
$\bar{I}_a^{\mathrm{ref}}, \bar{I}_b^{\mathrm{ref}}, \bar{I}_c^{\mathrm{ref}}$	reference currents to be drawn by the STATCOM;
V_{network}	positive sequence network voltage magnitude;
$P_{\mathrm{ref}}, Q_{\mathrm{ref}}$	reference STATCOM active and reactive power;
x_{comp}	equivalent SSSC reactance;
$\bar{V}_1, \bar{V}_2, \bar{V}_3$	SSSC injected series voltages;
$\bar{I}_1, \bar{I}_2, \bar{I}_3$	network line currents;
α	complement of the angle between $\bar{I}_a, \bar{I}_b, \bar{I}_c, [\bar{I}_1, \bar{I}_2, \bar{I}_3]$ and $\bar{V}_{ab}, \bar{V}_{bc}, \bar{V}_{ca}, [\bar{V}_1, \bar{V}_2, \bar{V}_3]$ for STATCOM [SSSC];

R_t, L_t, x_t coupling transformer leakage resistance, inductance, and reactance;

Kp_{ac}, Ki_{ac}
Kp_{dc}, Ki_{dc} PI regulators constant gains;

$L_{fA,k}, L_{fC,k}$ output filter inductances of k-th inverter;

C_{fA}, C_{fC} output filter capacitances;

$i_{fA,k}, i_{fC_k}$ output filter currents of k-th inverter;

i_{fA}, i_{fC} output filter capacitances currents;

$v_{dc,1}, v_{dc,2}$ dc voltages;

$u_{A,k}, u_{C,k}$ control input to k-th LC filter;

$u^+ = v_{dc,1}$ maximum positive voltage at LC filter input;

$u^- = -v_{dc,2}$ minimum negative voltage at LC filter input;

$s_{1,k}, s_{2,k}, s_{3,k}, s_{4,k}$ k-th inverter switches binary gate control signals;

$\mathbf{A}, \mathbf{B}, \mathbf{C}, \mathbf{D}$ matrices of state-space representation in (13);

$\Sigma(\mathbf{x}, t) = \mathbf{0}$ switching surface (17);

$\hat{\Sigma}(\mathbf{x}, t) = \mathbf{0}$ transformed switching surface (24).

APPENDIX B

Matrix Ω in (24) is given by (27)

$$\Omega = \left(\frac{\partial \Sigma}{\partial \mathbf{x}} \cdot \mathbf{B} \right)^{-1} \qquad (35)$$

where

$$\frac{\partial \Sigma}{\partial \mathbf{x}} \cdot \mathbf{B} = [\Gamma_1, \Gamma_2] \qquad (36)$$

and

$$\Gamma_1 = \begin{bmatrix} \frac{1}{L_{fA,n}} \frac{\partial \sigma_{A,1}}{\partial i_{fA,n}} & \cdots & \frac{1}{L_{fA,1}} \frac{\partial \sigma_{A,1}}{\partial i_{fA,1}} \\ \vdots & \ddots & \vdots \\ \frac{1}{L_{fA,n}} \frac{\partial \sigma_{A,n}}{\partial i_{fA,n}} & \cdots & \frac{1}{L_{fA,1}} \frac{\partial \sigma_{A,n}}{\partial i_{fA,1}} \\ \frac{1}{L_{fA,n}} \frac{\partial \sigma_{C,1}}{\partial i_{fA,n}} & \cdots & \frac{1}{L_{fA,1}} \frac{\partial \sigma_{C,1}}{\partial i_{fA,1}} \\ \vdots & \ddots & \vdots \\ \frac{1}{L_{fA,n}} \frac{\partial \sigma_{C,n}}{\partial i_{fA,n}} & \cdots & \frac{1}{L_{fA,1}} \frac{\partial \sigma_{C,n}}{\partial i_{fA,1}} \end{bmatrix} \qquad (37)$$

$$\Gamma_2 = \begin{bmatrix} \frac{1}{L_{fC,n}} \frac{\partial \sigma_{A,1}}{\partial i_{fC,n}} & \cdots & \frac{1}{L_{fC,1}} \frac{\partial \sigma_{A,1}}{\partial i_{fC,1}} \\ \vdots & \ddots & \vdots \\ \frac{1}{L_{fC,n}} \frac{\partial \sigma_{A,n}}{\partial i_{fC,n}} & \cdots & \frac{1}{L_{fC,1}} \frac{\partial \sigma_{A,n}}{\partial i_{fC,1}} \\ \frac{1}{L_{fC,n}} \frac{\partial \sigma_{C,1}}{\partial i_{fC,n}} & \cdots & \frac{1}{L_{fC,1}} \frac{\partial \sigma_{C,1}}{\partial i_{fC,1}} \\ \vdots & \ddots & \vdots \\ \frac{1}{L_{fC,n}} \frac{\partial \sigma_{C,n}}{\partial i_{fC,n}} & \cdots & \frac{1}{L_{fC,1}} \frac{\partial \sigma_{C,n}}{\partial i_{fC,1}} \end{bmatrix} \qquad (38)$$

TABLE I
STATCOM CONVERTER DATA

C_1, C_2	20 mF	$L_{fA,1}, L_{fC,1}$	5.0 mH
C_{fA}	2.55 mF	$L_{fA,2}, L_{fC,2}$	4.5 mH
C_{fC}	2.55 mF	$L_{fA,3}, L_{fC,3}$	4.0 mH

TABLE II
STATCOM PI CONTROLLER DATA

$K_{i,ac}$	500	$K_{i,dc}$	25
$K_{i,dc}$	5	$K_{i,dc}$	0.25

TABLE III
STATCOM SLIDING MODE CONTROLLER DATA

α	$2.0 \cdot 10^{-4}$	HB	5
β	0.3		

TABLE IV
SSSC CONVERTER DATA

C_1, C_2	10 mF	$L_{fA,1}, L_{fC,1}$	10 mH
C_{fA}	1 mF	$L_{fA,2}, L_{fC,2}$	11 mH
C_{fC}	1 mF	$L_{fA,3}, L_{fC,3}$	12 mH

TABLE V
SSSC PI CONTROLLER DATA

$K_{i,dc}$	50	$K_{i,dc}$	0.05

TABLE VI
SSSC SLIDING MODE CONTROLLER DATA

α	$2.0 \cdot 10^{-3}$	HB	1.5
β	1		

It results in

$$\frac{\partial \sigma_{A,j}}{\partial i_{fA,k}} = \begin{cases} \frac{\alpha}{C_{fA}}, & \text{if} \quad k \neq j, k \neq j-1 \\ \frac{\alpha}{C_{fA}} + \beta, & \text{if} \quad k = j \\ \frac{\alpha}{C_{fA}} - \beta, & \text{if} \quad k = j-1 \end{cases}$$

$$\frac{\partial \sigma_{A,j}}{\partial i_{fC,k}} = 0 \qquad (39)$$

and analogously

$$\frac{\partial \sigma_{C,j}}{\partial i_{fC,k}} = \begin{cases} \frac{\alpha}{C_{fC}}, & \text{if} \quad k \neq j, k \neq j-1 \\ \frac{\alpha}{C_{fC}} + \beta, & \text{if} \quad k = j \\ \frac{\alpha}{C_{fC}} - \beta, & \text{if} \quad k = j-1 \end{cases}$$

$$\frac{\partial \sigma_{C,j}}{\partial i_{fA,k}} = 0 \qquad (40)$$

APPENDIX C
DATA

STATCOM converter data used in simulations are given in Table I, while STATCOM controllers data are reported in Tables II and III.

SSSC converter data are given in Table IV, while SSSC controllers data are reported in Tables V and VI.

REFERENCES

[1] E. Acha, C. R. Fuerte-Esquivel, H. Ambriz-Perez, and C. Angeles-Camacho, *FACTS: Modelling and Simulation in Power Networks*. Chichester, U.K.: Wiley, 2004.

[2] V. K. Sood, *HVDC and FACTS Controllers. Applications of Static Converters in Power Systems*. Boston, MA: Kluwer, 2004.

[3] P. Moore and P. Ashmole, "Flexible AC transmission systems," *Power Eng. J.*, vol. 9, no. 6, pp. 282–286, Dec. 1995.

[4] P. Kundur, *Power System Stability and Control*. New York: McGraw-Hill, 1994.

[5] G. Rogers, *Power System Oscillations*. Boston, MA: Kluwer, 2000.

[6] L. Gyugyi, "Power electronics in electric utilities: Static VAR compensators," *Proc. IEEE*, vol. 76, no. 4, pp. 483–494, Apr. 1988.

[7] K. K. Sen, "STATCOM-STATic COMpensator: Theory, modeling and applications," *IEEE Trans. Power Del.*, vol. 2, no. 1, pp. 1177–1183, Feb. 1999.

[8] K. K. Sen, "SSSC-static synchronous series compensator: Theory, modeling and applications," *IEEE Trans. Power Del.*, vol. 13, no. 1, pp. 241–246, Jan. 1998.

[9] K. K. Sen and E. J. Stacey, "UPFC-unified power flow controller: Theory, modeling and applications," *IEEE Trans. Power Del.*, vol. 13, no. 4, pp. 1453–1460, Oct. 1998.

[10] L. Chen, Y. Liu, A. B. Arsoy, P. F. Ribeiro, M. Steurer, and M. R. Iravani, "Detailed modeling of superconducting magnetic energy storage (SMES) system," *IEEE Trans. Power Del.*, vol. 21, no. 2, pp. 699–710, Apr. 2006.

[11] D. Soto and T. C. Green, "A comparison of high-power converter topologies for the implementation of FACTS controllers," *IEEE Trans. Ind. Electron.*, vol. 49, no. 5, pp. 1072–1080, Oct. 2002.

[12] Y. Ye, M. Kazerani, and V. H. Quintana, "Current-source converter based STATCOM: Modeling and control," *IEEE Trans. Power Del.*, vol. 20, no. 2, pp. 795–800, Apr. 2005.

[13] A. H. Norouzi and A. M. Sharaf, "Two control schemes to enhance the dynamic performance of the STATCOM and SSSC," *IEEE Trans. Power Del.*, vol. 20, no. 1, pp. 435–442, Jan. 2005.

[14] M. S. El-Moursi and A. M. Sharaf, "Novel controllers for the 48-pulse VSC STATCOM and SSSC for voltage regulation and reactive power compensation," *IEEE Trans. Power Syst.*, vol. 20, no. 4, pp. 1985–1997, Nov. 2005.

[15] M. S. El-Moursi and A. M. Sharaf, "Novel reactive power controllers for the STATCOM and SSSC," *Electr. Power Syst. Res.*, vol. 76, no. 4, pp. 228–241, Jan. 2006.

[16] J. Rodriguez, J. S. Lai, and F. Z. Peng, "Multilevel inverters: A survey of topologies, controls, and applications," *IEEE Trans. Ind. Electron.*, vol. 49, no. 4, pp. 724–738, Aug. 2002.

[17] C. K. Lee, J. S. K. Leung, S. Y. R. Hui, and H. S.-H. Chung, "Circuit-level comparison of STATCOM technologies," *IEEE Trans. Power Electron.*, vol. 18, no. 4, pp. 1084–1092, Jul. 2003.

[18] P. K. Steimer, H. E. Grüning, J. Werninger, E. Carroll, S. Klaka, and S. Linder, "IGCT: A new emerging technology for high power, low cost inverter," in *Proc. 32nd Industrial Applications Soc. Annu. Meeting*, New Orleans, LA, Oct. 1997, vol. 2, pp. 1592–1599.

[19] P. K. Steimer, O. Apeldoorn, and E. Carroll, "IGCT devices—applications and future opportunities," in *Proc. IEEE Power Eng. Soc. Summer Meeting*, Seattle, WA, Jul. 2000, vol. 2, pp. 1223–1228.

[20] Y. Li, A. Q. Huang, and K. Motto, "Analysis of the snubberless operation of the emitter turn-off thyristor (ETO)," *IEEE Trans. Power Electron.*, vol. 18, no. 1, pp. 30–37, Jan. 2003.

[21] B. Zhang, A. Q. Huang, Y. Liu, and S. Atcitty, "Performance of the new generation emitter turn-off (ETO) thyristor," in *Proc. 37th IAS Annu. Meeting*, 2002, vol. 1, pp. 559–563.

[22] B. Zhang, A. Q. Huang, Y. Liu, B. Chen, and S. Atcitty, "SPETO: A superior power switch for high power, high frequency, low cost converters," in *Proc. 39th IAS Annu. Meeting*, Oct. 2004, vol. 3, pp. 1940–1946.

[23] J. Y. Hung, W. Gao, and J. C. Hung, "Variable structure control: A survey," *IEEE Trans. Ind. Electron.*, vol. 40, no. 1, pp. 2–22, Feb. 1993.

[24] R. A. DeCarlo, S. H. Zak, and G. P. Matthews, "Variable structure control of nonlinear multivariable systems: A tutorial," *Proc. IEEE*, vol. 76, no. 3, pp. 212–232, Mar. 1988.

[25] F. Blaabjerg, S. Freysson, H. H. Hansen, and S. Hansen, "A new optimized space-vector modulation strategy for a component-minimized voltage source inverter," *IEEE Trans. Power Electron.*, vol. 12, no. 4, pp. 704–714, Jul. 1997.

[26] E. Ledezma, B. McGrath, A. Munoz, and T. A. Lipo, "Dual AC-drive system with a reduced switch count," *IEEE Trans. Ind. Appl.*, vol. 37, no. 5, pp. 1325–1333, Sep. 2001.

[27] G. T. Kim and T. A. Lipo, "VSI-PWM rectifier-inverter system with a reduced switch count," *IEEE Trans. Ind. Appl.*, vol. 32, no. 6, pp. 1331–1337, Nov. 1996.

[28] B. R. Lin and T. C. Wei, "A novel NPC inverter for harmonics elimination and reactive power compensation," *IEEE Trans. Power Del.*, vol. 19, no. 3, pp. 1449–1456, Jul. 2004.

[29] V. I. Utkin, J. Guldner, and J. Shi, *Sliding Mode Control in Electromechanical Systems*. London, U.K.: Taylor & Francis, 1999.

[30] A. G. Loukianov, J. M. Canedo, V. I. Utkin, and J. Cabrera-Váazquez, "Discontinuous controller for power systems: Sliding-mode block control approach," *IEEE Trans. Ind. Electron.*, vol. 51, no. 2, pp. 340–353, Apr. 2004.

[31] V. I. Utkin, "Sliding mode control design principles and applications to electric drives," *IEEE Trans. Ind. Electron.*, vol. 40, no. 1, pp. 23–36, Feb. 1993.

[32] R. Ramos, D. Biel, F. Guinjoan, and E. Fossas, "Design considerations in sliding-mode controlled parallel-connected inverters," *in Proc. IEEE ISCAS*, no. 4, pp. 357–360, 2002.

[33] M. Carpita and M. Marchesoni, "Experimental study of a power conditioning system using sliding mode control," *IEEE Trans. Power Electron.*, vol. 11, no. 5, pp. 731–742, Sep. 1996.

[34] H. Sira-Ramirez, "Sliding motions in bilinear switched networks," *IEEE Trans. Circuits Syst.*, vol. 34, no. 8, pp. 919–933, Aug. 1987.

Antonio Griffo was born in Torino, Italy, in 1978. He received the Master's degree in electronic engineering and the Ph.D. degree in electrical engineering from the University of Naples "Federico II", Naples, Italy, in 2003 and 2007, respectively.

Currently, he is a Research Associate at the University of Sheffield, Sheffield, U.K., working on power system stability analysis for the More Electric Aircraft. His research interests include modeling, and stability analysis and control of power systems and power electronics.

Davide Lauria received the electrical engineering degree (Hons.) and the Master's degree in mathematics (Hons.) from the University of Naples "Federico II," Naples, Italy, in 1987 and 1995, respectively.

He is a Full Professor in the Electrical Engineering Department, University of Naples. His research areas include power systems stability and power-electronics applications in power systems.